PCCP

PAPER

View Article Online
View Journal | View Issue

Cite this: *Phys. Chem. Chem. Phys.*, 2025, **27**, 22386

Partial atomic charge of oxygen and hydrogen-bonding ability: insights from mass-selective IR spectroscopy of jet-cooled hydrogen-bonded complexes†

Akshay Kumar Sahu,[ab] Anant Ram Satpathi,[ab] Saiprakash Rout,[ab] Radharaman Samanta,[ab] Laxmipriya Dash[ab] and Himansu S. Biswal *[ab]

Received 25th August 2025,
Accepted 28th September 2025

DOI: 10.1039/d5cp03250d

rsc.li/pccp

The hydrogen bond is a fundamental non-covalent interaction that underpins the structure and function of chemical and biological systems. While the nature of conventional hydrogen bonding is predominantly electrostatic, accurately describing the atomic charge distribution within molecules remains a significant challenge, as atomic charges are not physically observable quantities. In this work, we present a systematic experimental investigation of hydrogen bonding in the gas phase using mass-selective IR spectroscopy of jet-cooled *p*-cresol–acceptor dimers. The redshift of the *p*-cresol OH stretching frequency ($\Delta\nu_{OH}$) serves as a direct measure of hydrogen-bond strength. We analysed two series of acceptors, acyclic alcohols and ethers, which demonstrate increasing inductive effects, and cyclic ethers, which reveal the influence of resonance. The gas-phase spectroscopy results provide a dataset that serves as a benchmark for validating computational chemistry models used for atomic charge calculation. It was demonstrated that while standard hydrogen-bonding descriptors correlate well with the experimental data, many popular partial atomic charge models fail to reproduce the observed chemical trends. This failure could be due to the over-reliance of the models on the electronegativity of directly bonded atoms. By highlighting this discrepancy, this work serves as a valuable cautionary example regarding the use of atomic charges and underscores the need for better theoretical frameworks for atomic charge estimation.

Introduction

The hydrogen bond (H-bond) is one of the most important non-covalent interactions in chemistry and biology.[1,2] Its strength and directionality govern molecular recognition, drive protein folding, and dictate the structure of liquid water.[3–5] The nature of conventional H-bonds, such as O–H···O, O–H···N, is predominantly electrostatic,[6,7] meaning that their strengths are highly dependent on the charge distribution of the interacting molecules.[8,9] For this reason, computational models of H-bonded systems, such as force fields for molecular dynamics simulations, heavily rely on the concept of partial atomic charges (PAC).[10–12] While indispensable for modelling, PACs are not physically observable.[13] Their calculation from a quantum-mechanical wavefunction is a fundamentally ambiguous process, and over 50 different methodologies have been proposed since Mulliken's pioneering work in 1955.[14–18] This proliferation of methods highlights the lack of a universal, physically rigorous approach. For computational chemists, this raises a crucial question: which method best reproduces experimental reality? Extensive efforts have been made to validate PAC models using theoretical parameters.[19–24] Direct experimental benchmarks remain rare. One notable example is the work of R. J. Lovelock in 2018.[25] Lovelock employed X-ray photoelectron spectroscopy (XPS) and near-edge X-ray absorption fine structure (NEXAFS) spectroscopy to investigate atomic charges on nitrogen atoms in nine ionic liquids. However, the relationship between computed charges and experimentally measurable properties remains poorly established.

Gas-phase spectroscopy of isolated, jet-cooled complexes provides an ideal experimental method to address this question. The absence of a solvent enables a direct study of the intrinsic properties of a H-bond, free from external influence.[26–29] In this study, we use resonance-ion-dip infrared (RIDIR) spectroscopy to measure the OH stretching frequency

[a] *School of Chemical Sciences, National Institute of Science Education and Research (NISER), PO-Bhimpur-Padanpur, Via-Jatni, District-Khurda, PIN - 752050, Bhubaneswar, India. E-mail: himansu@niser.ac.in*
[b] *Homi Bhabha National Institute, Training School Complex, Anushakti Nagar, Mumbai 400094, India*

† Dedicated to Professor Resnati, celebrating a career in fluorine and noncovalent chemistry on the occasion of his 70th birthday

redshift ($\Delta\nu_{OH}$) of H-bonded *p*-cresol (*p*CR) dimers. The magnitude of this redshift serves as a direct, sensitive probe of the H-bond strength, which is itself proportional to the electron-donating ability (or the electron density) of the acceptor molecule, making this interaction an ideal testbed for evaluating PAC models.[30–32]

Herein, this experimental technique has been used to investigate two distinct series of hydrogen-bond acceptors: (I) cyclic ethers: this series includes furan (FRN), 2,3-dihydrofuran (2,3-DHF), 2,5-dihydrofuran (2,5-DHF), and tetrahydrofuran (THF). These molecules allow us to investigate the role of resonance and conjugation on the electron density of the acceptor oxygen within a five-membered ring structure. (II) Acyclic alcohols and ethers: This series includes water (H_2O), methanol (MeOH), ethanol (EtOH), iso-propanol (^{i}PrOH), *t*-butanol (*t*BuOH), dimethyl ether (DME), diethyl ether (DEE), and di-isopropyl ether (DIE). We chose these molecules to systematically probe how increasing alkyl substitution, which is a well-documented source of inductive electron-donating effects, influences electron density at the oxygen and thus the H-bond strength.[33,34] By combining these two experimental series, we build a comprehensive dataset that serves as a benchmark for evaluating computational PAC models.

In this work, we systematically evaluate 18 widely used charge assignment schemes, including Hirshfeld,[35] Voronoi deformation density (VDD),[36] Mulliken,[14–16] Löwdin,[37] Modified Mulliken by Ros & Schuit (SCPA),[38] Modified Mulliken by Stout & Politzer (SP),[39] Modified Mulliken by Bickelhaupt (Bickel),[40] Becke,[41] Atomic Dipole Corrected Hirshfeld (ADCH),[42] CHELPG,[43] Merz–Kollmann (M–K),[44] Charge Model-5 (CM5),[45] RESP,[46] electronegativity equalization method (EEM),[47] partial equalization of orbital electronegativity (PEOE),[48,49] minimal basis iterative stockholder (MBIS),[50] natural population analysis (NPA),[51] and Bader's atoms in molecules (AIM).[52] While the experimental data provide clear, chemically intuitive trends, it can be shown that many widely used computational charge models fail to reproduce these same trends. This work does not aim to propose a new charge model; instead, it uses the experimental data to clearly demonstrate the limitations of existing charge methodologies and serves as a cautionary example for non-experts.

Results and discussion

Experimental trends in hydrogen-bonding strength

To probe the strength of H-bonding, we employed supersonic jet-cooled, mass-selective IR (RIDIR) spectroscopy. RIDIR spectra were obtained by introducing IR photons 50–100 ns prior to UV excitation and ionisation. The UV excitation frequency was fixed at 35 331 cm^{-1} for the *p*CR monomer, while for the *p*CR dimers with cyclic ethers, the frequencies were 35 119 cm^{-1} (pCR–FRN), 34 925 cm^{-1} (*p*CR–2,3-DHF), 34 756 cm^{-1} (*p*CR–2,5-DHF), and 34 849 cm^{-1} (*p*CR–THF). For the alcohol dimers, the corresponding excitation frequencies were 34 974, 34 906, 34 909, 34 952, and 34s935 cm^{-1} for H_2O, MeOH, EtOH, ^{i}PrOH, and tBuOH, respectively. For the acyclic ethers, the excitation frequencies were 34 871 cm^{-1} (DME), 34 880 cm^{-1} (DEE), and 34 839 cm^{-1} (DIE). The ionisation frequency for the 2C-R2PI spectra was fixed at 37 700 cm^{-1}. The corresponding mass-selective REMPI spectra are shown in Fig. S1–S3.

The redshift of the *p*CR OH stretching frequency ($\Delta\nu_{OH}$) from its monomer value of 3658 cm^{-1} provides a reliable measure of H-bond strength. For the cyclic five-membered ethers (Fig. 1a–e), the observed order of H-bond strength, based on $\Delta\nu_{OH}$, is chemically intuitive: FRN (-78 cm^{-1}) < 2,3-DHF (-188 cm^{-1}) < 2,5-DHF (-282 cm^{-1}) < THF (-318 cm^{-1}). This trend directly reflects the degree of conjugation of the oxygen lone pair. In FRN, the oxygen lone pair is fully conjugated with two double bonds, which significantly reduces its electron density and H-bonding ability. In 2,3-DHF, the conjugation with a single double bond weakens this effect, while in 2,5-DHF, the double bond is not conjugated with the oxygen, leaving a higher electron density on the oxygen. Finally, in THF, the oxygen lone pair is fully localised and available for bonding, making it the strongest acceptor.

For the acyclic alcohols and ethers, the H-bond strength also follows a well-established trend that is consistent with the increasing electron-donating inductive effect of the alkyl groups. The corresponding $\Delta\nu_{OH}$ values are -127, -191, -217, -241, and -257 cm^{-1} for the alcohol series (H_2O, MeOH, EtOH, ^{i}PrOH, and tBuOH, respectively), as shown in Fig. 1f–k. For the ether series, the redshifts are -127, -242, -280, and -303 cm^{-1} for the corresponding dimers with H_2O, DME, DEE, and DIE (Fig. 1l–p). This data confirms that the H-bond strength increases with the electron-donating ability of the substituents. It is important to note that previous studies by some of us have reported the *p*CR–H_2O,[53] *p*CR–MeOH,[54] *p*CR–EtOH,[54] and *p*CR–DEE dimers,[55] and our current results are in excellent agreement with those works, validating our experimental setup.

Computational analysis of H-bonding strength and atomic charges

The validation of the experimental data was carried out by comparing it to established theoretical descriptors of H-bond strength. Quantum-chemical calculations were performed to evaluate the OH···O bond length, binding energy, QTAIM electron density at the bond critical point (ρ(BCP)), and NBO donor–acceptor interaction energy (E(2)). The values are given in Table S1.

For cyclic ethers, all parameters, *i.e.*, the OH···O bond length, binding energy, BCP electron density, and E(2), show excellent linear correlations with $\Delta\nu_{OH}$, with R^2 values of 0.963, 0.982, 0.994, and 0.990, respectively (Fig. 2a–d). This confirms that the experimental frequency shift is a reliable indicator of H-bond strength. For the alcohols and acyclic ethers, similar correlations were observed, except in the case of the binding energy (R^2 = 0.700); the other parameters gave R^2 values of 0.916 (bond length), 0.904 (BCP electron density), and 0.816 (E(2)) (Fig. 2g–j). Again, these results validate $\Delta\nu_{OH}$ as a consistent probe of H-bonding strength. The molecular graph generated

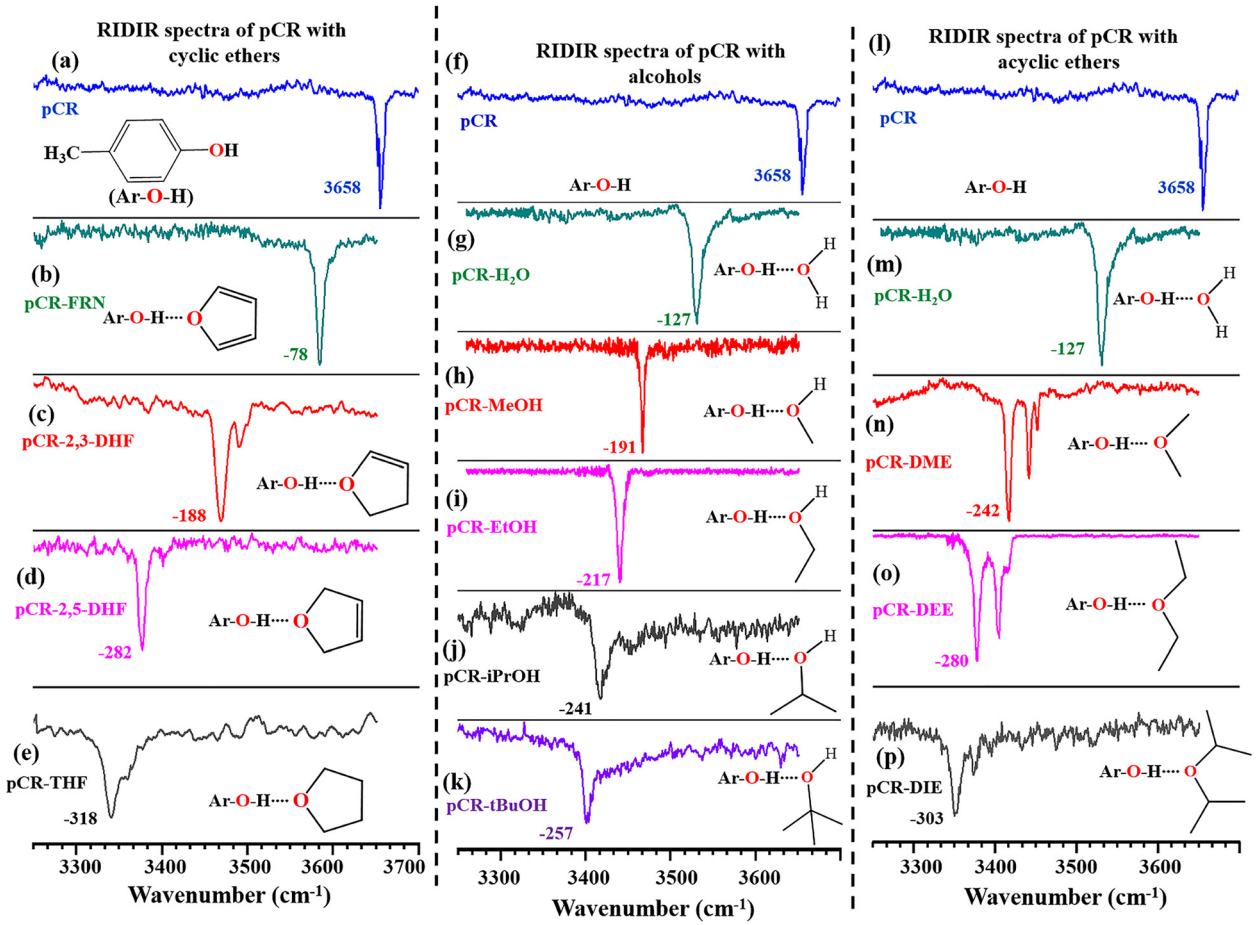

Fig. 1 Mass-selected vibrational spectra (RIDIR spectra) of Left Panel: H-bonded dimers of *p*CR with cyclic ethers, including (b) *p*CR–FRN, (c) *p*CR–2,3-DHF, (d) *p*CR–2,5-DHF, and (e) *p*CR–THF; Middle Panel: H-bonded dimers of *p*CR with alcohols, including (g)–(k) *p*CR with H_2O, MeOH, EtOH, ^{i}PrOH, and tBuOH, respectively; Right Panel: H-bonded dimers of *p*CR with acyclic ethers, including (m)–(p) *p*CR with H_2O, DME, DEE, and DIE, respectively. For comparison, the RIDIR spectrum of the *p*CR monomer is included at the top of each panel. The RIDIR spectra for the *p*CR–H_2O, *p*CR–MeOH, *p*CR–EtOH, and *p*CR–DEE dimers have been previously reported in the literature; the experiments were reproduced here, yielding similar results.[53–55]

from QTAIM analysis and the donor–acceptor natural orbital generated from NBO analysis are shown in Fig. S4 and S5, respectively.

To probe the nature of the interactions, SAPT2 energy decomposition analysis was performed, which confirmed that the OH···O hydrogen bonds were predominantly electrostatic in nature (Fig. S6). The values of the different components of SAPT2 analysis are given in Table S2. The strong correlation between the electrostatic contribution and $\Delta\nu_{OH}$, with R^2 values of 0.987 for cyclic ethers (Fig. 2e) and 0.955 for alcohols and acyclic ethers (Fig. 2k), further reinforces the idea that our $\Delta\nu_{OH}$ values are a direct measure of the electron density on the oxygen atom.

The molecular electrostatic potential (MESP) at the oxygen atom was calculated and compared with the $\Delta\nu_{OH}$. The MESP values are given in Table S1. The MESP maps of the molecules are shown in Fig. S7. For the cyclic ethers, which share a common molecular backbone, the MESP values correlated strongly with the shifts (R^2 = 0.988; Fig. 2f). However, a perplexing anomaly emerged for the acyclic systems: the alcohols exhibited higher MESP values (more negative potential) on the oxygen than the ethers. This trend is counter-intuitive given the expected stronger inductive effect from the alkyl groups in ethers (Fig. 2l). The computed PACs on the oxygen atom for cyclic and acyclic systems, obtained using 18 different population analysis schemes, are given in Tables 1 and 2, respectively. Because different methods yield different charge trends, we first screened these methods using the cyclic ether data, which showed consistent H-bonding trends. Among the tested methods, the ADCH, CM5, and PEOE charges exhibited the most consistent correlations with H-bond strength (Table S3) and were therefore chosen for further analysis owing to their robustness and widespread applicability.[56–58]

The computed charges were plotted against the experimental $\Delta\nu_{OH}$ values. As shown in Fig. 3, the cyclic ethers exhibit strong linear correlations between the IR shifts and the PACs of oxygen obtained from ADCH, CM5, and PEOE (Fig. 3a–c). In these systems, a more negative oxygen charge corresponds to a larger IR redshift, which is expected. This provided an initial indication that these methods could correctly capture the

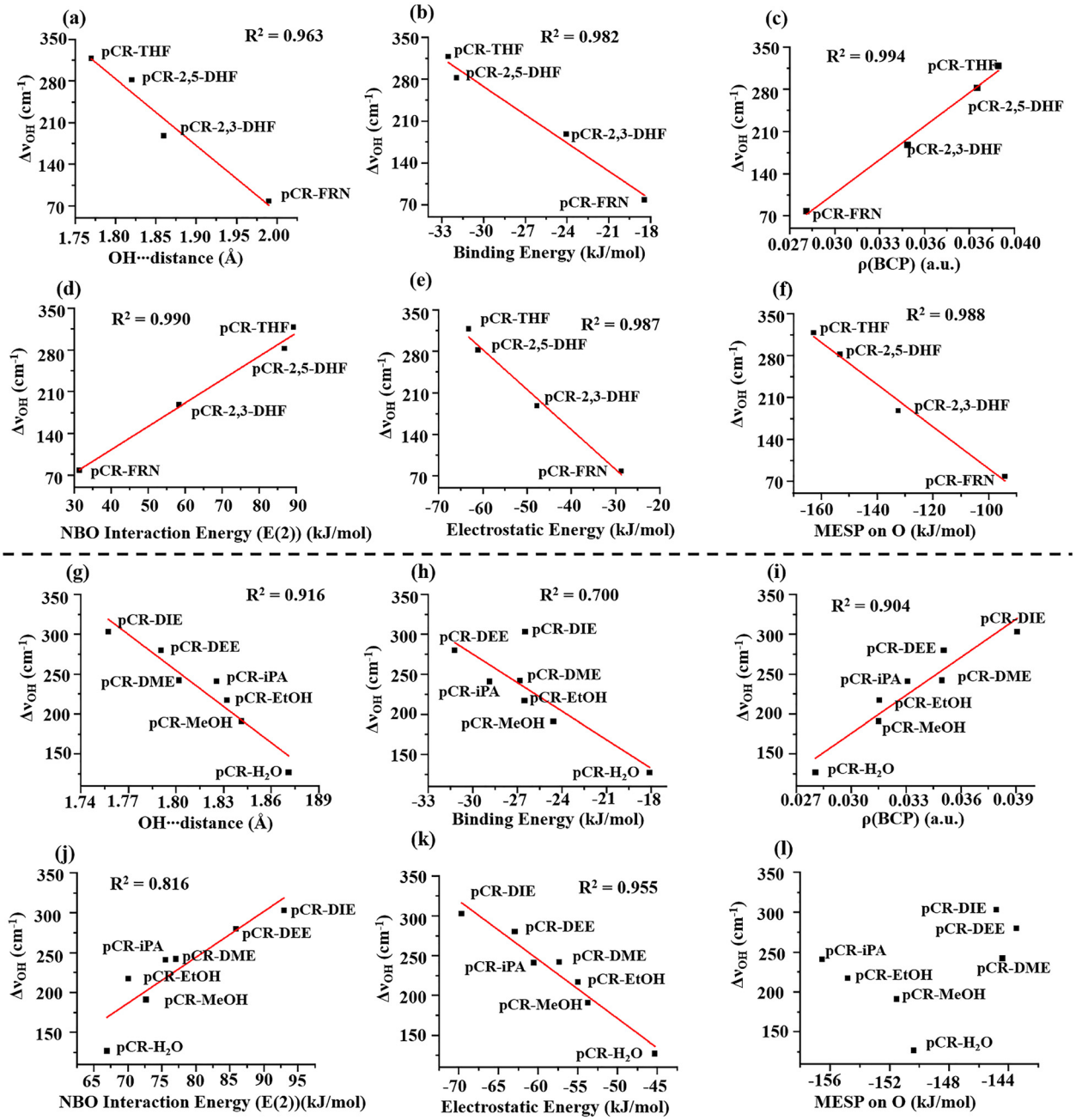

Fig. 2 Correlation plots between the redshift of the *p*CR OH stretching frequency ($\Delta\nu_{OH}$) with various H-bond descriptors such as OH···O bond length, binding energy, ρ(BCP), NBO interaction energy (E(2)), electrostatic energy contribution, and MESP on oxygen for Top panel: (a)–(f) H-bonded complexes with cyclic ethers and Bottom panel: (g)–(l) H-bonded complexes with alcohols and acyclic ethers.

charge trends. However, when we applied these same charge models to the acyclic alcohols and ethers, the correlations failed. Despite the clear experimental trend of increasing H-bond strength with increasing alkyl substitution, the computed oxygen charges often became less negative; the ethers consistently display the least-negative charges, followed by alcohols, with water exhibiting the most-negative oxygen charge (Fig. 3d–f). This trend is in stark contradiction to the experimental data, in which the H-bond strength increases from water to alcohols to ethers. This result serves as a cautionary example. It demonstrates that many widely used computational charge models, while mathematically sound, can produce charges that are inconsistent with fundamental, experimentally validated trends. This is particularly problematic for non-experts who might use these models without fully understanding their limitations.

Inclusion of electronegativity corrections

The ADCH and CM5 charges show different slopes for different alkyl groups, whereas PEOE yields nearly identical slopes for all

Table 1 Partial atomic charges (PAC) of oxygen for cyclic ethers (FRN, 2,3-DHF, 2,5-DHF, and THF) obtained at the MP2/aug-cc-pVDZ level of theory

	FRN	2,3-DHF	2,5-DHF	THF
Hirshfeld	−0.142	−0.207	−0.226	−0.228
VDD	−0.166	−0.252	−0.273	−0.275
Mulliken	−0.715	−0.897	−0.929	−0.911
Löwdin	0.075	0.020	0.007	0.000
SCPA	−0.985	−0.685	−0.860	−1.232
SP	−0.919	−1.039	−0.941	−0.892
Bickel	−0.760	−0.837	−0.943	−0.844
Becke	−0.338	−0.389	−0.476	−0.476
ADCH	−0.164	−0.246	−0.309	−0.324
CHELPG	−0.153	−0.311	−0.585	−0.466
MK	−0.114	−0.268	−0.546	−0.425
CM5	−0.220	−0.291	−0.316	−0.323
RESP	−0.114	−0.268	−0.543	−0.423
PEOE	−0.326	−0.354	−0.373	−0.381
MIBS	−0.254	−0.400	−0.466	−0.455
EEM	−0.550	−0.539	−0.522	−0.528
NPA	−0.580	−0.667	−0.689	−0.688
AIM	−1.072	−1.055	−1.023	−1.038

three types of alkyl group (Fig. 3d–f). This suggests that the electronegativity of the atoms bonded to the oxygen atoms plays some role, as the PEOE methods calculate atomic charges by partially equalising the orbital electronegativity of the atoms.[48,49] This is again supported by the fact that the average electronegativity difference (ΔEN) between oxygen and its bonded atoms is approximately 1.24 for water (O–H bond), 1.06 for alcohols (O–C and O–H), and 0.89 for ethers (O–C bonds).

As presented in Table 2, larger ΔEN values consistently correspond to more-negative computed oxygen charges, which explains why water consistently shows the most negative charge across different models, despite being the weakest H-bond acceptor in this series.

To further illustrate the dominant influence of electronegativity, empirical adjustments were introduced to the computed charges. A correction was first applied based on the electronegativity difference ΔEN_1 between the central oxygen and the atoms directly bonded to it (eqn (2)–(4)).

$$Q_X^{\mathrm{Corr}\prime} = Q_X - q'_X \quad (1)$$

$$q'_{\mathrm{ADCH}} = -1.46\Delta EN_1 + 1.13 \quad (2)$$

$$q'_{\mathrm{CM5}} = -1.13\Delta EN_1 + 1.00 \quad (3)$$

$$q'_{\mathrm{PEOE}} = -0.2\Delta EN_1 + 0.17 \quad (4)$$

where ΔEN_1 is the difference between the electronegativity of the atom and the average electronegativity of the atoms directly bonded to it (position one) and q'_X is the correction parameter for X = ADCH, CM5 and PEOE.

This adjustment significantly improved the correlations with $\Delta\nu_{OH}$ (Fig. 4a–c); the only significant deviations were observed for MeOH, DME, and ^{i}PrOH, DIE and *t*-BuOH, which may be attributed to the fact that in these molecules, the central atom is bonded to a $-CH_3$, $-C_3H_7$ and $-C_4H_9$ group, respectively, whereas EtOH and DEE have a $-C_2H_5$ group, similar to FRN, 2,3-DHF, 2,5-DHF, and THF. To address these cases, we refined the correction by incorporating the average electronegativity of more distal substituents (EN_{av}; Eqn5).

$$Q_X^{\mathrm{Corr}} = Q_X - q_X \quad (5)$$

$$q_{\mathrm{ADCH}} = -1.24\Delta EN_1 - 0.03(EN_C - EN_{av}) + 1.11 \quad (6)$$

$$q_{\mathrm{CM5}} = -1.04\Delta EN_1 - 0.01(EN_C - EN_{av}) + 0.92 \quad (7)$$

$$q_{\mathrm{PEOE}} = -0.14\Delta EN_1 - 0.01(EN_C - EN_{av}) + 0.12 \quad (8)$$

The variable q_X in eqn 5 represents the modified charge, where X = ADCH, CM5 and PEOE, EN_C refers to the electronegativity of the carbon atom (2.55), and EN_{av} is the average electronegativity of the other atoms at all positions other than position one. The values of EN_1 and EN_{av} are provided in Table S4. Electronegativity (EN) calculations for various

Table 2 Partial atomic charges (PAC) of oxygen for alcohols (MeOH, EtOH, ^{i}PrOH, tBuOH) and acyclic ethers (DME, DEE and DIE) obtained at the MP2/aug-cc-pVDZ level of theory

	H_2O	MeOH	EtOH	^{i}PrOH	*t*BuOH	DME	DEE	DIE
Hirshfeld	−0.312	−0.267	−0.270	−0.271	−0.268	−0.215	−0.211	−0.214
VDD	−0.286	−0.292	−0.292	−0.296	−0.288	−0.273	−0.264	−0.267
Mulliken	−0.315	−0.611	−0.687	−0.748	−0.679	−0.830	−0.924	−1.052
Löwdin	0.169	0.071	0.097	0.118	0.136	−0.049	0.006	0.044
SCPA	−0.383	−0.953	−0.891	−0.708	−0.154	−1.507	−1.444	−0.787
SP	−0.621	−0.769	−0.880	−0.899	−1.207	−0.858	−0.683	−0.782
Bickel	−0.338	−0.600	−0.696	−0.742	−1.125	−0.785	−0.758	−1.298
Becke	−0.707	−0.603	−0.647	−0.689	−0.726	−0.416	−0.525	−0.632
ADCH	−0.707	−0.519	−0.515	−0.505	−0.487	−0.317	−0.291	−0.289
CHELPG	−0.725	−0.644	−0.694	−0.719	−0.772	−0.379	−0.491	−0.618
MK	−0.720	−0.632	−0.689	−0.713	−0.748	−0.314	−0.474	−0.581
CM5	−0.642	−0.486	−0.485	−0.482	−0.476	−0.324	−0.313	−0.307
RESP	−0.719	−0.631	−0.687	−0.710	−0.746	−0.314	−0.468	−0.573
PEOE	−0.411	−0.400	−0.397	−0.394	−0.391	−0.388	−0.382	−0.376
MIBS	−0.897	−0.662	−0.683	−0.693	−0.688	−0.414	−0.438	−0.467
EEM	−0.642	−0.591	−0.602	−0.608	−0.613	−0.526	−0.538	−0.544
NPA	−0.963	−0.808	−0.812	−0.814	−0.823	−0.686	−0.701	−0.709
AIM	−1.203	−1.120	−1.124	−1.122	−1.122	−1.063	−1.070	−1.064

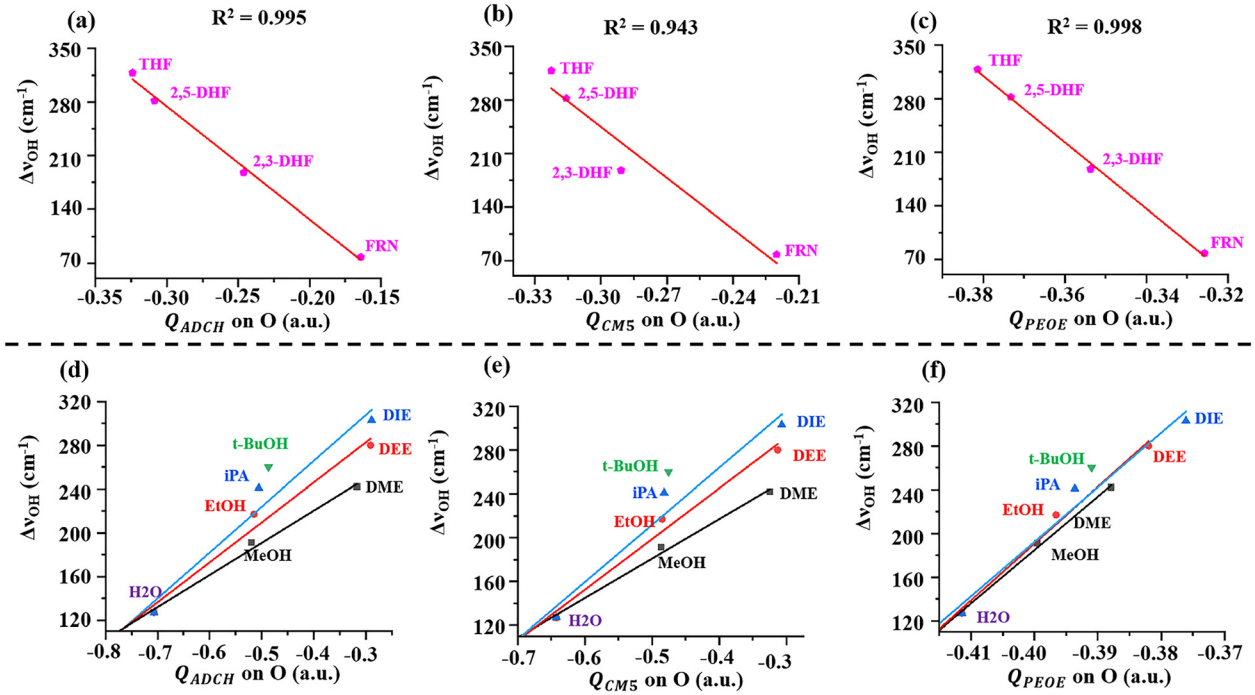

Fig. 3 Correlation plots between the atomic charges and the redshift of the *p*CR OH stretching frequency ($\Delta\nu_{OH}$). Top panel: (a)–(c) $\Delta\nu_{OH}$ *vs.* uncorrected ADCH, CM5, and PEOE charges for H-bonded dimers with cyclic ethers (FRN, 2,3-DHF, 2,5-DHF, and THF); Bottom panel: (d)–(f) $\Delta\nu_{OH}$ *vs.* uncorrected ADCH, CM5, and PEOE charges for H-bonded dimers with alcohols and acyclic ethers.

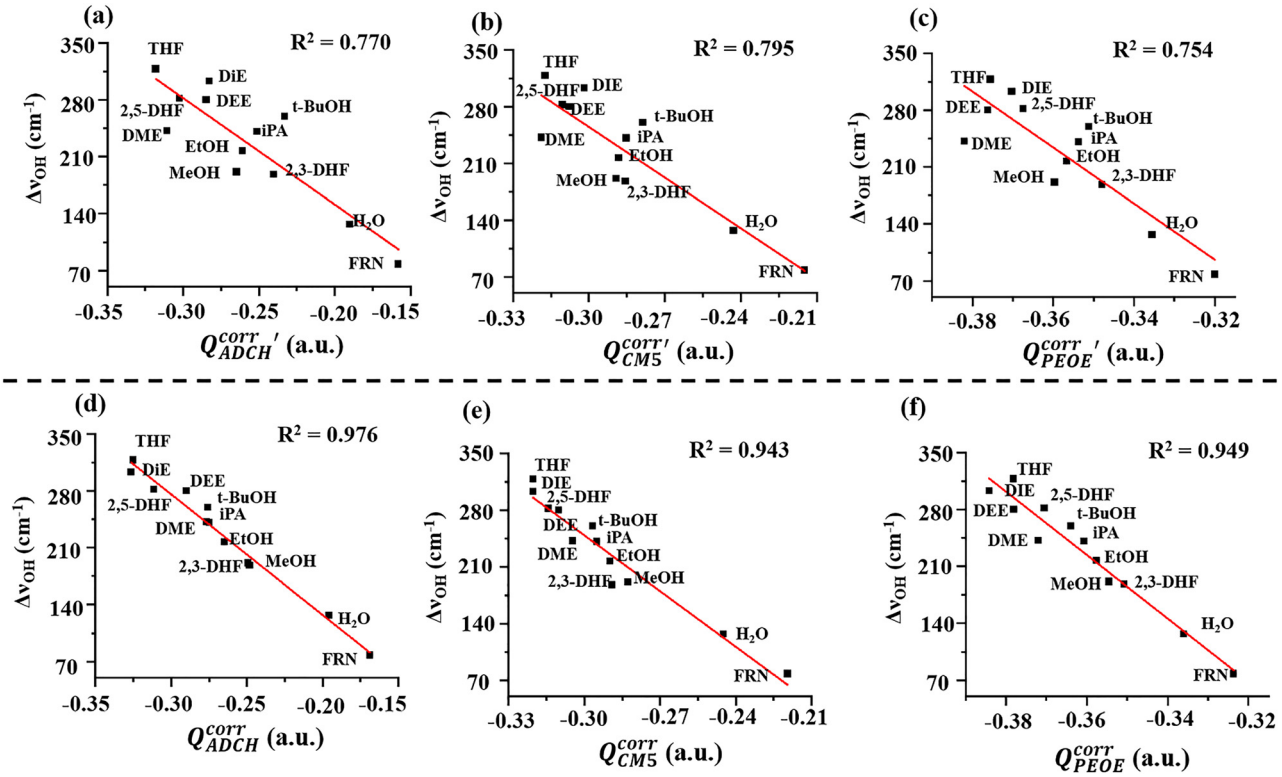

Fig. 4 Correlation plots between corrected atomic charges and redshift of the *p*CR OH stretching frequency ($\Delta\nu_{OH}$) of H-bonded dimers. Top panel: (a)–(c) $\Delta\nu_{OH}$ *vs.* ΔEN_1-corrected charges obtained from ADCH $\left(Q^{Corr'}_{ADCH}\right)$, CM5 $\left(Q^{Corr'}_{CM5}\right)$, and PEOE $\left(Q^{Corr'}_{PEOE}\right)$, Bottom panel: (d)–(f) $\Delta\nu_{OH}$ *vs.* ΔEN_{av}-corrected charges obtained from ADCH (Q^{Corr}_{ADCH}), CM5 (Q^{Corr}_{CM5}), and PEOE (Q^{Corr}_{PEOE}).

molecules were carried out using the molecular structures shown in Fig. S9. The molecule DEE was chosen as the reference, as FRN, 2,3-DHF, 2,5-DHF, and THF all share the same backbone. This molecule contains three distinct positions. At position 1, the central oxygen atom is bonded to two carbon atoms, giving EN_1 = 2.55. At position 2, six atoms (two carbons and four hydrogens) are present, resulting in EN_2 = 2.32. At position 3, six hydrogen atoms are present, giving EN_3 = 2.20 (Fig. S9a). The average electronegativity is therefore EN_{av} = 2.26. A more detailed explanation of the other molecules, the determination of these quantities, and the procedure used to derive the equations (eqn 2–4 and 6–8) are provided in the SI.

This refined, multi-parameter adjustment incorporating both ΔEN_1 and the average electronegativity of the surrounding atoms (EN_{av}) yielded a marked improvement in the correlation between the computed atomic charges and the experimental $\Delta\nu_{OH}$ shifts (Fig. 3d–f), achieving R^2 values of 0.976, 0.943, and 0.949 for ADCH, CM5, and PEOE, respectively. The unadjusted, ΔEN_1-adjusted, and EN_{av}-adjusted charges for ADCH, CM5, and PEOE are summarised in Tables S5–S7. Among these, the ADCH method shows the strongest linear correlation after adjustment.

To demonstrate the generality of this effect, we extended the analysis to nitrogen-containing systems (NH_3, diethylamine (DEA), triethylamine (TEA)) for which the gas-phase IR spectra were available.[59] Experimental gas-phase basicity trends and $\Delta\nu_{OH}$ shifts for the H-bonded complexes of these compounds with phenol reveal that TEA is a stronger hydrogen-bond acceptor and more basic than DEA, while NH_3 is the weakest.[60] However, the unadjusted ADCH charges predicted the opposite trend. When the influence of ΔEN was incorporated using the empirical relation given in eqn (S5), the corrected ADCH charges agreed with the experimental observations (Fig. S8), reinforcing the consistent impact of electronegativity across different classes of H-bond acceptors. This result is also consistent with the observations of Snurr *et al.*,[23] who found that the PAC model is more dependent on directly bonded atoms, with a secondary yet significant contribution from distal atoms.

The ability to ''fix'' the models by accounting for a simple, fundamental property, such as electronegativity, highlights that the underlying algorithms of these models are not correctly capturing the electronic distribution in a chemically intuitive manner.

Conclusions

In this work, a comprehensive experimental dataset of H-bonding in the gas phase has been presented, which provides a benchmark for evaluating quantum chemical models. The systematic investigation of both cyclic and acyclic acceptors reveals clear, intuitive H-bonding strength trends. However, comparing these data with 18 popular charge calculation methods reveals a poor correlation between the computed atomic charges of the H-bond acceptors and the corresponding H-bond strengths, particularly for systems such as the OH···O H-bonding examples studied in the present work, which involve various substituents. These findings serve as a critical warning: many widely used charge models are inherently biased by the electronegativity of bonded atoms, leading them to produce results that contradict well-established chemical principles and experimental observations. This highlights the need for caution when using these models and underscores the importance of experimental validation. This manuscript offers a high-quality dataset that can be used to develop and test new theoretical frameworks, which will ultimately contribute to the creation of more physically meaningful atomic charges, which will be essential for accurately modelling a vast range of chemical phenomena.

Author contributions

Conceptualization: HSB, methodology: HSB, AKS, ARS, investigation: AKS, ARS, SR, RS, LD, HSB, visualization: AKS, ARS, SR, RS, LD, HSB, funding acquisition: HSB, project administration: HSB, supervision: HSB, writing: original draft: AKS, HSB, writing: review & editing: AKS, ARS, SR, RS, LD, HSB

Conflicts of interest

There are no conflicts to declare.

Data availability

The data supporting this work are uploaded as part of the supplementary information (SI). Supplementary information is available. See DOI: **https://doi.org/10.1039/d5cp03250d**.

Acknowledgements

A. K. S., A. R. S, S. R., R. S., L. D., and H. S. B. acknowledge financial support from the Department of Atomic Energy, Anusandhan National Research Foundation (ANRF) (Project File No: CRG/2022/001096), Govt. of India.

Notes and references

1 G. A. Jeffrey, *An introduction to hydrogen bonding*, Oxford university press New York, 1997.
2 E. Arunan, G. R. Desiraju, R. A. Klein, J. Sadlej, S. Scheiner, I. Alkorta, D. C. Clary, R. H. Crabtree, J. J. Dannenberg and P. Hobza, *Pure Appl. Chem.*, 2011, **83**, 1637–1641.
3 L. Pauling and R. B. Corey, *Proc. Natl. Acad. Sci. U. S. A.*, 1951, **37**, 251–256.
4 C. N. Pace, H. Fu, K. Lee Fryar, J. Landua, S. R. Trevino, D. Schell, R. L. Thurlkill, S. Imura, J. M. Scholtz and K. Gajiwala, *Prot. Sci.*, 2014, **23**, 652–661.
5 F. H. Stillinger, *Science*, 1980, **209**, 451–457.

6 S. Scheiner, *Hydrogen bonding: a theoretical perspective*, Oxford University Press, 1997.
7 K. Morokuma and K. Kitaura, Chemical Applications of Atomic and Molecular Electrostatic Potentials: Reactivity, *Structure, Scattering, and Energetics of Organic, Inorganic, and Biological Systems*, Springer, 1981, pp. 215–242.
8 T. Steiner, *Angew. Chem., Int. Ed.*, 2002, **41**, 48–76.
9 G. R. Desiraju and T. Steiner, *The weak hydrogen bond: in structural chemistry and biology*, International Union of Crystal, 2001.
10 J. Wang, R. M. Wolf, J. W. Caldwell, P. A. Kollman and D. A. Case, *J. Comput. Chem.*, 2004, **25**, 1157–1174.
11 S. J. Weiner, P. A. Kollman, D. A. Case, U. C. Singh, C. Ghio, G. Alagona, S. Profeta and P. Weiner, *J. Am. Chem. Soc.*, 1984, **106**, 765–784.
12 A. D. MacKerell Jr, *J. Comput. Chem.*, 2004, **25**, 1584–1604.
13 J. Meister and W. H. E. Schwarz, *J. Phys. Chem.*, 1994, **98**, 8245–8252.
14 R. S. Mulliken, *J. Chem. Phys.*, 1955, **23**, 1833–1840.
15 R. S. Mulliken, *J. Chem. Phys.*, 1955, **23**, 1841–1846.
16 R. S. Mulliken, *J. Chem. Phys.*, 1955, **23**, 2338–2342.
17 T. Lu and Q. Chen, *Exploring Chemical Concepts Through Theory and Computation*, 2024, pp. 161–188.
18 T. Lu and F.-W. Chen, *Acta Phys. – Chim. Sin*, 2012, **28**, 1–18.
19 B. Wang, S. L. Li and D. G. Truhlar, *J. Chem. Theory Comput.*, 2014, **10**, 5640–5650.
20 T. A. Manz and D. S. Sholl, *J. Chem. Theory Comput.*, 2010, **6**, 2455–2468.
21 J. Zhao, Z.-W. Zhu, D.-X. Zhao and Z.-Z. Yang, *Phys. Chem. Chem. Phys.*, 2023, **25**, 9020–9030.
22 K. B. Wiberg and P. R. Rablen, *J. Org. Chem.*, 2018, **83**, 15463–15469.
23 S. Kancharlapalli, A. Gopalan, M. Haranczyk and R. Q. Snurr, *J. Chem. Theory Comput.*, 2021, **17**, 3052–3064.
24 K. B. Wiberg and P. R. Rablen, *J. Comput. Chem.*, 1993, **14**, 1504–1518.
25 R. M. Fogarty, R. P. Matthews, C. R. Ashworth, A. Brandt-Talbot, R. G. Palgrave, R. A. Bourne, T. Vander Hoogerstraete, P. A. Hunt and K. R. J. Lovelock, *J. Chem. Phys.*, 2018, **148**, 193817.
26 Y. Yamada, T. Ebata, M. Kayano and N. Mikami, *J. Chem. Phys.*, 2004, **120**, 7400–7409.
27 T. Ebata, A. Iwasaki and N. Mikami, *J. Phys. Chem. A*, 2000, **104**, 7974–7979.
28 S. Kumar, P. Biswas, I. Kaul and A. Das, *J. Phys. Chem. A*, 2011, **115**, 7461–7472.
29 S. Ghosh, P. Chopra and S. Wategaonkar, *Phys. Chem. Chem. Phys.*, 2020, **22**, 17482–17493.
30 D. Cheshmedzhieva, S. Ilieva, B. Hadjieva and B. Galabov, *J. Phys. Org. Chem.*, 2021, **34**, e4258.
31 B. Galabov, V. A. Popov, D. Cheshmedzhieva, S. Ilieva and H. F. Schaefer Iii, *Chem. Phys. Lett.*, 2022, **791**, 139378.
32 A. K. Sahu, A. R. Satpathi, S. Rout, P. Mohanty, L. Dash and H. S. Biswal, *J. Phys. Chem. Lett.*, 2024, **15**, 11445–11453.
33 J. Clayden, *Organic Chemistry*, 2nd edn, Oxford University Press, Oxford, 2012.
34 R. A. Benkeser, R. A. Hickner and D. I. Hoke, *J. Am. Chem. Soc.*, 1958, **80**, 2279–2282.
35 F. L. Hirshfeld, *Theor. Chim. Acta*, 1977, **44**, 129–138.
36 C. Fonseca Guerra, J.-W. Handgraaf, E. J. Baerends and F. M. Bickelhaupt, *J. Comput. Chem.*, 2004, **25**, 189–210.
37 P. O. Löwdin, *J. Chem. Phys.*, 1950, **18**, 365–375.
38 P. Ros and G. C. A. Schuit, *Theor. Chim. Acta*, 1966, **4**, 1–12.
39 E. W. Stout and P. Politzer, *Theor. Chim. Acta*, 1968, **12**, 379–386.
40 F. M. Bickelhaupt, N. J. R. van Eikema Hommes, C. Fonseca Guerra and E. J. Baerends, *Organometallics*, 1996, **15**, 2923–2931.
41 A. D. Becke, *J. Chem. Phys.*, 1988, **88**, 2547–2553.
42 T. Lu and F. Chen, *J. Theor. Comput. Chem.*, 2012, **11**, 163–183.
43 C. M. Breneman and K. B. Wiberg, *J. Comput. Chem.*, 1990, **11**, 361–373.
44 B. H. Besler, K. M. Merz Jr and P. A. Kollman, *J. Comput. Chem.*, 1990, **11**, 431–439.
45 A. V. Marenich, S. V. Jerome, C. J. Cramer and D. G. Truhlar, *J. Chem. Theory Comput.*, 2012, **8**, 527–541.
46 J. Wang, P. Cieplak and P. A. Kollman, *J. Comput. Chem.*, 2000, **21**, 1049–1074.
47 W. J. Mortier, K. Van Genechten and J. Gasteiger, *J. Am. Chem. Soc.*, 1985, **107**, 829–835.
48 J. Gasteiger and M. Marsili, *Tetrahedron Lett.*, 1978, **19**, 3181–3184.
49 J. Gasteiger and M. Marsili, *Tetrahedron*, 1980, **36**, 3219–3228.
50 T. Verstraelen, S. Vandenbrande, F. Heidar-Zadeh and L. Vanduy, *J. Chem. Theory Comput.*, 2016, **12**, 3894–3912.
51 A. E. Reed, R. B. Weinstock and F. Weinhold, *J. Chem. Phys.*, 1985, **83**, 735–746.
52 R. F. W. Bader, *Atoms In Molecules: A Quantum Theory*, Clarendon Press, Oxford, UK, 1990.
53 H. S. Biswal, P. R. Shirhatti and S. Wategaonkar, *J. Phys. Chem. A*, 2009, **113**, 5633–5643.
54 H. S. Biswal, P. R. Shirhatti and S. Wategaonkar, *J. Phys. Chem. A*, 2010, **114**, 6944–6955.
55 H. S. Biswal and S. Wategaonkar, *J. Phys. Chem. A*, 2010, **114**, 5947–5957.
56 Y. Fu, H. Liu, B. Z. Tang and Z. Zhao, *Nat. Commun.*, 2023, **14**, 2019.
57 Y. Yuan, L. Zhou, H. Robatjazi, J. L. Bao, J. Zhou, A. Bayles, L. Yuan, M. Lou, M. Lou, S. Khatiwada, E. A. Carter, P. Nordlander and N. J. Halas, *Science*, 2022, **378**, 889–893.
58 G. M. Morris, R. Huey, W. Lindstrom, M. F. Sanner, R. K. Belew, D. S. Goodsell and A. J. Olson, *J. Comput. Chem.*, 2009, **30**, 2785–2791.
59 A. Iwasaki, A. Fujii, T. Watanabe, T. Ebata and N. Mikami, *J. Phys. Chem.*, 1996, **100**, 16053–16057.
60 J. I. Brauman, J. M. Riveros and L. K. Blair, *J. Am. Chem. Soc.*, 1971, **93**, 3914–3916.